Current Science
CS 5 (4), 3914-3924 (2025)
Received 16 May 2025 | **Revised 12 June** 2025 | **Accepted 13July**. 2025 | **Online Available 11 August** 2025
https://doi.org/ 10.52845/CS/2025-5-4-48

Current Science

Current Science

OPEN ACCESS

ISSN(O)2795-8639

Original Article

Inverse Modeling of Electrified Road Surface Roughness Based on Vehicle Dynamic Response

Libo Yuan[1], Wei Zhou[1], Huifu Jiang[1*], Yongjian Ma[1], Lu zhang[1]

[1]Research Institute of Highway Ministry of Transport, Beijing 100088, China

[*]Corresponding Author: Huifu Jiang

Abstract:
To support the analysis of vibration excitation characteristics in electrified road systems, this study proposes an inverse modeling approach for reconstructing road surface roughness in heavy-duty transport scenarios based on vehicle dynamic responses. The method segments the measured suspension displacement signal using RMS values in the time domain and initializes road profile parameters using a parameterized harmonic superposition model. Road spectrum strength and spectral characteristics are iteratively optimized in each segment by minimizing the RMS error between simulated and measured responses, ultimately generating a 3D roughness model of the road surface. To assess the engineering applicability of the reconstructed model, a frequency-domain analysis is conducted on the translational and rotational excitations at the pantograph base. Results reveal that pitch and vertical responses dominate in the low-frequency range and exhibit strong coupling, whereas roll and lateral responses show multi-peak characteristics in the mid- to high-frequency range, indicating possible local resonance phenomena. This research provides a novel methodology and theoretical basis for modeling complex road surfaces and their application in the dynamic analysis of electrified highway systems.

Keywords: Road Roughness, Inverse Modeling, Vehicle Response, Electrified Road

Introduction

As the global transportation sector shifts toward cleaner energy sources, electrified roads—integrating renewable energy and intelligent power delivery—are emerging as a promising solution for heavy-duty freight transport. These systems enable continuous high-power energy supply via onboard pantographs drawing current from overhead contact lines, eliminating the need for traditional fueling or frequent charging [1,2].

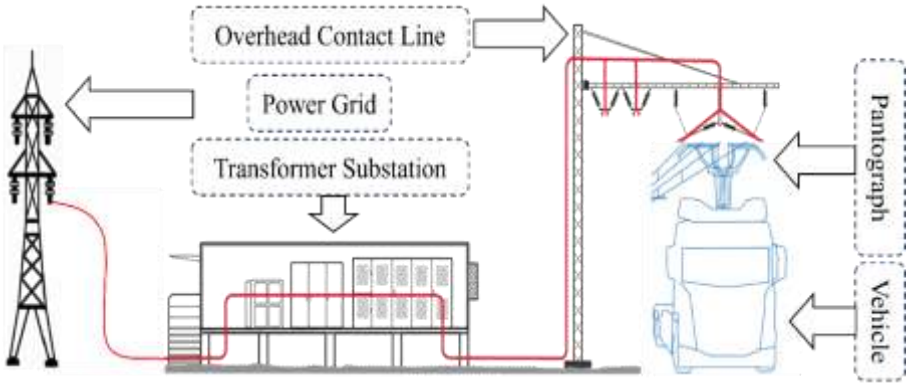

Figure 1.Electrified Roads schematic diagram

However, prolonged operation under heavy loads leads to road degradation, including rutting, subsidence, and localized damage [3,4]. These surface irregularities induce significant vehicle dynamic responses, resulting in fluctuating excitations at the pantograph base and reduced quality of pantograph–catenary interaction. This places higher demands on onboard sensor systems (e.g., for image stabilization), the precision of active pantograph control, and vehicle structural layout. Addressing these challenges requires accurate and representative modeling of real-world heavy-duty road roughness conditions.

Road roughness is typically obtained using either direct measurement or reconstruction methods. While measurement offers high accuracy, it is often constrained by site accessibility and incurs significant time and equipment costs. In contrast, reconstruction methods estimate road roughness by transforming power spectral density (PSD) into spatial profiles. These methods are widely used due to their simplicity and flexibility, with common techniques including the harmonic superposition method [5,6], white noise modeling [7-9], and inverse Fourier transform [10]. However, traditional reconstruction approaches are generally tailored for standard road classes and fail to capture the complexities of continuous, non-uniform road surfaces. Consequently, they are inadequate for reproducing the realistic dynamic responses of vehicles on complex terrain. To address this, various vehicle response–based road identification techniques have been developed, including machine learning algorithms [11,12], and transfer function approaches [13,14]. However, each method has limitations: machine learning depends heavily on hyperparameter tuning and input selection, and high-order transfer function models often suffer from convergence issues.

To address the limitations of conventional modeling techniques, this paper presents a novel inverse modeling approach that reconstructs road surface roughness from vehicle dynamic responses. As an engineering application, the proposed method is employed to analyze the excitation behavior of the pantograph base on uneven electrified roads, providing practical insights for system design and control.

2 Methods

The inverse road roughness model based on vehicle response is a regional modeling approach that combines response inversion with parameter iteration and optimization. By analyzing the vehicle displacement response spectrum and incorporating a three-dimensional harmonic superposition road model, this method enables reverse fitting of the actual road segment's 3D roughness profile. The modeling procedure is illustrated in **Figure 2**.

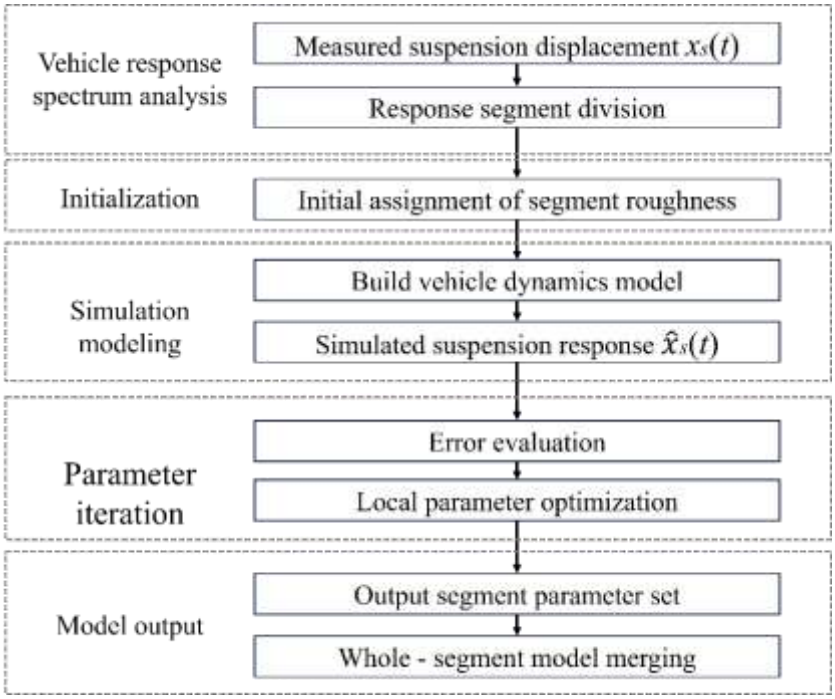

Figure 2 Flowchart of the inverse modeling process for road roughness

2.1 Analysis of Vehicle Response Spectrum

The vertical response intensity of a vehicle over a given road segment is closely correlated with the strength of road excitation. Therefore, segments with higher root mean square (RMS) values typically indicate regions with more severe road roughness.After conducting the driving test over the target road section, the vertical displacement time-history signal at the suspension is extracted. Following denoising and preprocessing, the local RMS values are computed using the following equation.

$$RMS = \sqrt{\frac{1}{T}\int_0^T x_i(t)^2 dt} \qquad (1)$$

Based on the temporal variations in response intensity, segments exhibiting significant changes are identified and selected as modeling subregions for subsequent inverse reconstruction. The number of segments can be flexibly adjusted based on the desired modeling accuracy in the analysis.

2.2 Initial Assumption of Road Spectrum

The harmonic superposition method is based on the theory of stationary random processes and approximates a stochastic road surface characterized by a specific power spectral density (PSD) using a series of superimposed harmonic components. Each harmonic component has defined attributes such as frequency, wavelength, amplitude, and phase, allowing for straightforward conversion of experimental data into model parameters. This approach offers high controllability, interpretability, and stable statistical properties, making it well suited for inverse modeling of road roughness.

The target road segment is treated as an independent modeling unit. An initial estimate of the road class for this segment is made based on empirical knowledge, and a corresponding power spectral density function is reconstructed using the harmonic superposition principle:

$$G_q(n) = G_q(n_0)\left(\frac{n}{n_0}\right)^{-w} \qquad (2)$$

Where $G(n_i)$ and $G_q(n)$ denote the road power spectral density, $G_q(n_0)$ is the reference PSD at spatial frequency n_0, n_i is the i discrete spatial frequency, Δn is the frequency interval, $\phi_i \in [0,2\pi]$ are independently and uniformly distributed phase angles, and w is the waviness exponent.

The 3D random road roughness profile is then synthesized within the target frequency range using the harmonic superposition method:

$$z(x,y) = \sum_{i=1}^{N_x}\sum_{j=1}^{N_y}\sqrt{2G(n_{xi},n_{yj})\Delta n_x \Delta n_y}\cdot\cos\left(2\pi(n_{xi}x + n_{yj}y) + \phi_{ij}\right) \qquad (3)$$

Where $z(x,y)$ represents the road elevation at point (x,y), and $G(n_x,n_y)$ denotes the three-dimensional PSD. The modeled road roughness within the same segment must satisfy both isotropic and anisotropic conditions: that is, the roughness properties should be directionally dependent—relatively rougher in the longitudinal direction and smoother in the lateral direction. The corresponding PSD function is required to meet the following conditions.

$$G(n_x,n_y) = G\left(\sqrt{n_x^2 + n_y^2}\right) \qquad (4)$$

$$G(n_x, n_y) = G_0 \cdot \left(\frac{\sqrt{(n_x)^2 + \lambda^2 (n_y)^2}}{n_0} \right)^{-w} \qquad (5)$$

where λ represents the statistical anisotropy factor that characterizes directional differences in roughness. When λ>1, the contribution of spatial frequency in the y to the power spectral density is amplified, indicating more pronounced roughness features laterally. When λ<1, the influence of the y is diminished, and the roughness features are more dominant in the longitudinal x direction. When λ=1, the PSD depends solely on the radial spatial frequency, implying isotropic surface characteristics with no distinction between the x and y directions.

2.3 Simulation and Error Evaluation

The initial road roughness profile is used as the excitation input to the vehicle dynamic model to compute the simulated vehicle response $\hat{x}s(t)$. The simulated displacement response $\hat{x}s(t)$ is then compared against the measured data $x_s(t)$ for error evaluation. In the time domain, the root mean square error (RMSE) of displacement is used as the metric for accuracy assessment.

$$RMSE_{\hat{x}_s} = \sqrt{\frac{1}{T}\int_0^T \left[x_s(t) - \hat{x}_s(t) \right]^2 dt} \qquad (6)$$

2.4 Local Parameter Iteration

To minimize the discrepancy between simulated and measured responses, the road spectrum parameters for the current segment must be iteratively optimized. As described above, the key parameter set for the harmonic superposition road roughness model include:

$$P = \left\{ G_d(n_0), n_{min}, n_{max}, \Delta x, \Delta y, w \right\} \qquad (7)$$

where $G_q(n_0)$ represents the spectral intensity at the reference spatial frequency and determines the overall excitation energy of the profile. n_{min} and n_{max} define the lower and upper bounds of the spatial frequency range, which control the effective excitation bandwidth. The frequency range should be gradually expanded to encompass the natural frequencies of heavy-duty vehicles. Δx and Δy represent the spatial sampling resolution in the longitudinal and lateral directions, respectively, which affect simulation accuracy. Smaller sampling intervals are required as spatial frequency increases. The parameter w controls the attenuation rate of high-frequency components; reducing w can enhance road roughness in cases where the surface is overly smooth. After each parameter update, the simulation and error evaluation process (as described in **Section 1.3**) is repeated until the error converges.

2.5 Global Model Output

Once all local segment models pass the error validation, they are sequentially concatenated to form a continuous road surface model for the entire section. To address potential discontinuities or abrupt changes at the junctions between segments, specific harmonic components are superimposed locally during the merging process. This smooths out local irregularities and ensures continuity of the overall roughness profile.

$$z_w(x, y) = z(x, y) + \sum_j \sqrt{2G(n_j)\Delta n}\, e^{\left(-\frac{(x-x_j)^2}{2\sigma_{xj}^2} - \frac{(y-y_j)^2}{2\sigma_{yj}^2} \right)} \cos(2\pi n_j x) \qquad (8)$$

In this formulation, $z(x, y)$ represents the base road roughness, while the second term introduces a localized disturbance to capture abrupt surface transitions. This perturbation is implemented using a cosine wave modulated by a Gaussian

window function, enabling spatial localization. The Gaussian window confines the effect of the disturbance to the vicinity of x_j, rapidly attenuating to zero as the distance from x_j increases. Specifically, the window function reaches its maximum value of 1 at $x=x_j$, where the disturbance is fully applied. When $|x-x_j|>3\sigma_j$, as the window function approaches zero, the disturbance becomes negligible.

3 Acquisition of Vehicle Response Spectrum

To reconstruct road roughness profiles from vehicle responses, it is necessary to acquire motion response data from heavy-duty vehicles operating on heavily loaded roadways. Coal transport roads near mining areas serve as typical examples of heavily loaded roadways. Prolonged operation of heavy-duty vehicles on these roads results in various forms of surface degradation, closely resembling the long-term road profile conditions seen in electrified road systems for freight transport. A coal transport corridor near a coal mine in Lüliang, Shanxi Province, was selected as the test site. Response data were collected from a four-axle heavy-duty dump truck operating along this corridor. Measurements included axle-end accelerations and suspension displacements. The data acquisition setup is shown in **Figure 3**.

A. Six-component force sensor B. Pull wire displacement sensor C. Acceleration sensor

Figure 3Vehicle response data acquisition equipment

Accelerometers were mounted on the axle ends and just above the axle heads. Cable-type displacement sensors were installed at each suspension unit, with one end attached to the axle and the other to the vehicle body directly above, allowing for direct measurement of time-varying suspension displacement.

During the measurement run, the dump truck traveled from a short stretch of loess road within the mining area to surrounding asphalt roads, encountering various conditions such as uphill and downhill segments. Since overhead contact lines in electrified roads can be installed discontinuously, data from complex segments where installation is unnecessary were excluded. The 460–490 s segment features a continuous and consistent road surface, making it suitable for validating the inverse modeling approach.

● The suspension displacement of the third axle was selected as the response signal. The time-history curve of the left suspension on the third axle is shown in

Figure 4.

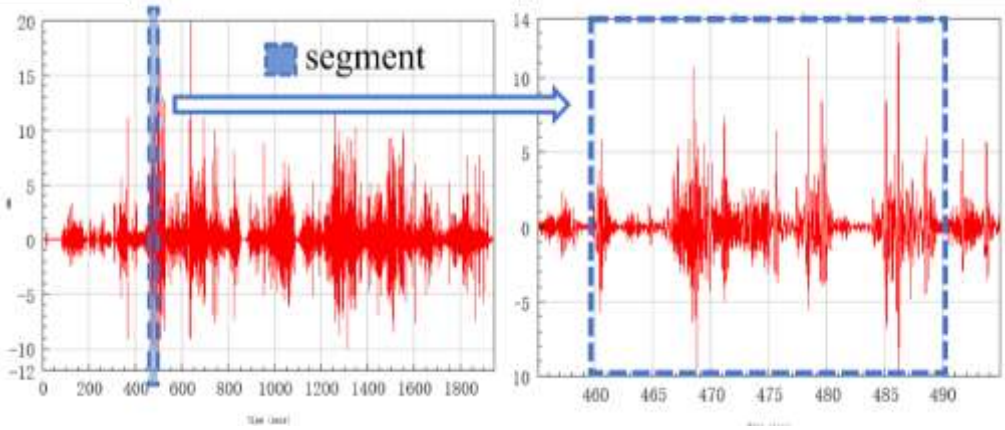

Figure 4 the displacement of the left suspension of the third axis before and after slicing

A comparison between the 460–490 s segment and the entire asphalt road section revealed similar frequency-domain characteristics and power spectral density (PSD) distributions. Thus, this segment is representative of typical asphalt roads under heavy-duty operation. The frequency spectrum of the vertical acceleration at the third axle's left wheel, obtained using fast Fourier transform (FFT), is shown in **Figure 5**.

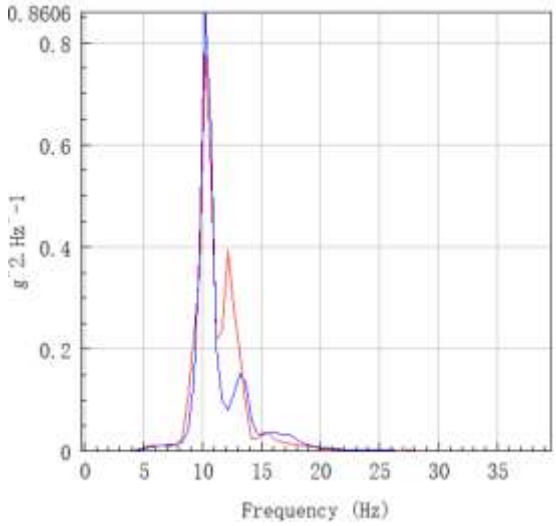

Figure 5 Frequency-domain distribution of the third axle's left suspension displacement before and after segment slicing

4 Model Validation

To verify the effectiveness of the proposed inverse modeling approach, the measured displacement of the third axle's left suspension is used as input. The reconstructed three-dimensional road profile is then applied to drive a vehicle dynamics simulation model, and the simulated dynamic response at the corresponding vehicle location is compared against the measured data for error analysis.

The response spectrum of the left suspension on the dump truck's third axle was segmented based on local root mean square (RMS) values, resulting in five distinct segments, as shown in **Figure 6.**

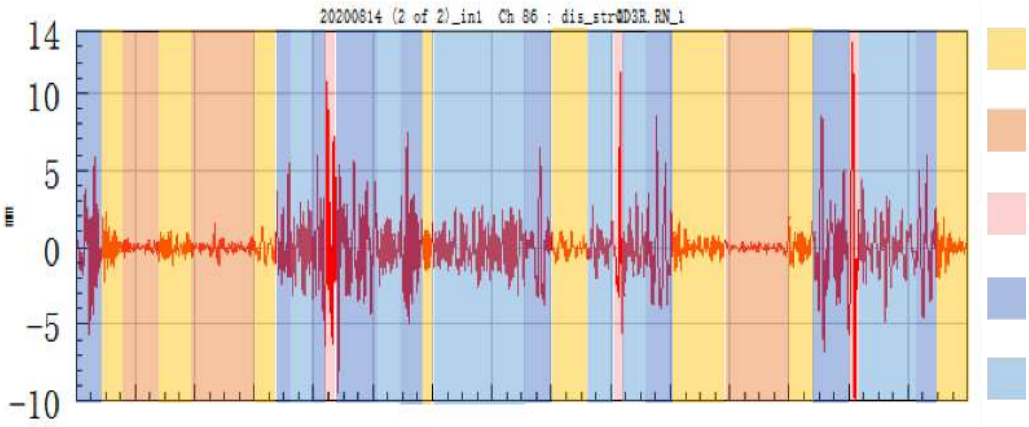

Figure 6 Suspension response segmentation results

Initially, the five segments were assumed to correspond to B, C, D, E, and F level road roughness, based on the relative magnitude of the suspension displacement responses. To evaluate the accuracy of the assumed segment-wise road roughness, an initial roughness profile was configured using TruckSim. To minimize interference from other factors, a dynamic model of the four-axle dump truck was reconstructed in TruckSim using the measured vehicle parameters and recorded driving speeds. The vehicle model and speed settings are shown in **Figure 7**.

A1. The vehicle models established in Trucksim

B1. Testing dump truck

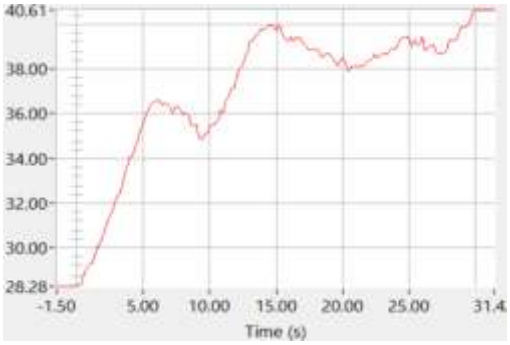

A2. The vehicle speed in Trucksim

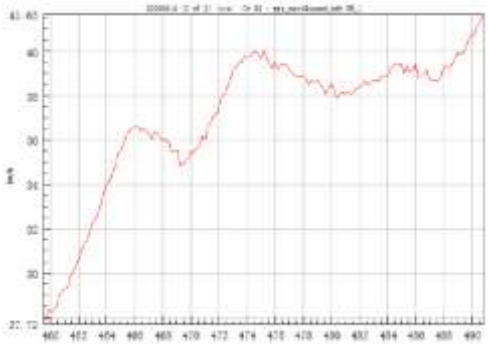

B2. Measured speed

Figure 7 Vehicle dynamics simulation modeling

Following iterative parameter optimization, the suspension displacement errors across all segments converged. The final harmonic superposition model parameters for each segment are summarized in Error! Reference source not found..Given the vehicle speed range of v=7.86~11.28m/s, the corresponding spatial frequency bounds ensure a time-domain frequency range of f=0.0786~56.4Hz, which sufficiently covers the natural frequencies of both sprung and unsprung masses in heavy-duty vehicles [17].

Table 1 The set of modeling parameters for the harmonic superposition of each section

Section	$G_0(q)$ $(10^{-6}m^3)$	n_{max}	n_{min}	w	Δx (m)	Δy (m)	Proportion
	8~32	5	0.1	2	0.2	0.1	42.08%
	128~512	5	0.01	2	0.2	0.1	4.70%
	128~512	5	0.1	1.8	0.2	0.1	37.28%
	521~2048	5	0.05	1.8	0.2	0.1	2.92%
	521~2048	5	0.1	1.6	0.2	0.1	13.02%

The simulation results for the third axle are presented as an example. A comparison between the measured and simulated vertical suspension displacements on both sides of the third axle is shown in **Figure 8**

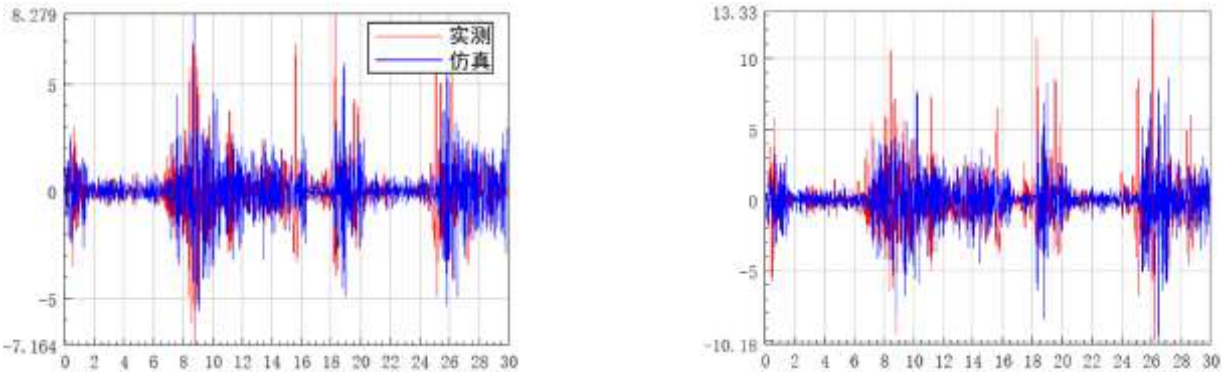

A. Left suspension B. Right suspension

Figure 8 Comparison of measured and simulated results for vertical displacement of the third axis's left and right suspensions

The amplitude distributions of the left and right suspension displacements on the third axle are illustrated in **Figure 9**.

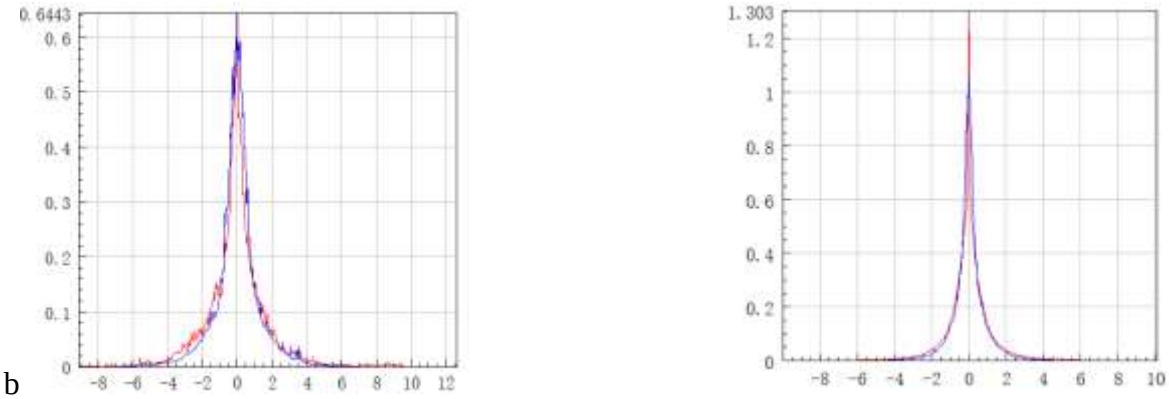

b

B. Left suspension B. Right suspension

Figure 9 Comparison of displacement amplitude distribution for the third axis's left and right rear suspensions

In addition to suspension displacement, the RMS of body acceleration serves as a key indicator of overall vibration intensity. The calculated RMS acceleration values for the left and right suspensions on the third axle are listed in Table **2**.

Table 2 Comparison of characteristic values of acceleration data from the left and right suspensions of the third axis

Components	Data	RMS	Mean Value
Left suspension	Measured acceleration	1.543	−2.139×10−4
	Simulation acceleration	1.611	1.041×10−3
Right suspension	Measured acceleration	1.761	−1.448×10−3
	Simulation acceleration	1.709	1.16×10−4

A comparison of measured and simulated data confirms that the reconstructed road roughness, obtained via the suspension response-based inverse modeling approach, effectively captures the actual characteristics of heavy-duty road surfaces.

5 Engineering Application

Building upon the reconstructed heavy-duty road surface model, its practical applicability is examined through an engineering case study. Given the direct impact of pantograph base excitation on the quality of pantograph–catenary interaction, a preliminary investigation is conducted to characterize the dynamic excitation behavior at the pantograph base.

In practice, the onboard DCDC converter (DCDC) is rigidly mounted to the tractor frame, and the pantograph is installed on top of the DCDC unit. Therefore, the displacement at the top of the DCDC serves as the direct excitation source for the pantograph during vehicle operation. A dynamic model of the electrified tractor was reconstructed in TruckSim, where the combined mass of the DCDC and pantograph assembly was represented by a 2.3-ton mass block, as illustrated in Figure 10**.**

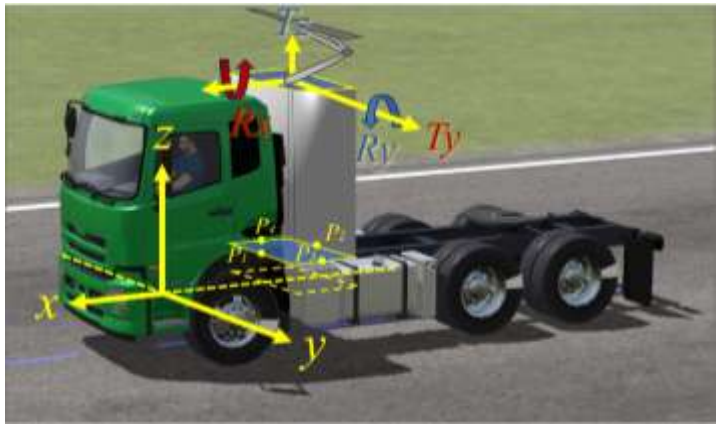

Figure 10 Electric tractor modle

To obtain the input motion response at the pantograph base, we define P_i (x_i, y_i, z_i) as a characteristic point on the tractor where the transport-induced motion spectrum varies. This point is defined in the vehicle coordinate system and can be determined through simulation. The onboard DCDC unit is modeled as a rigid body. The excitation acting on the pantograph base is decomposed into translational and rotational components. Yaw rotation R_z and longitudinal translation T_x are neglected due to their minimal influence. Accordingly, the displacement of any point on the rigid body can be expressed by the following equation:

$$\begin{cases} dy = T_y - R_x \cdot z_i \\ dz = T_z + R_x \cdot y_i - R_y \cdot x_i \end{cases} \quad (9)$$

Where, *dy* and *dz* denote the displacements of a point in the lateral (Y) and vertical (Z) directions, respectively; *Ty* and *Tz* represent the translational motion of the rigid body along the Y and Z axes; *Rx* and *Ry* are the rotation angles of the rigid body about the X and Y axes; and (x_i, y_i, z_i) is the

initial coordinate of the point in the vehicle coordinate system.

For each time step *t*, the displacement measurements in the Y and Z directions at point P_i are used to solve for the motion parameters *Ty*, *Tz* , *Rx*, and *Ry*.

$$\mathbf{A}\cdot\mathbf{X}=\mathbf{D} \qquad (10)$$

$$\mathbf{A}=\begin{bmatrix}1 & 0 & -z_1 & 0\\ 0 & 1 & y_1 & -x_1\\ 1 & 0 & -z_2 & 0\\ 0 & 1 & y_2 & -x_2\\ 1 & 0 & -z_3 & 0\\ 0 & 1 & y_3 & -x_3\\ 1 & 0 & -z_4 & 0\\ 0 & 1 & y_4 & -x_4\end{bmatrix},\quad \mathbf{X}=\begin{bmatrix}T_y\\ T_z\\ R_x\\ R_y\end{bmatrix},\quad \mathbf{D}=\begin{bmatrix}dy_1\\ dz_1\\ dy_2\\ dz_2\\ dy_3\\ dz_3\\ dy_4\\ dz_4\end{bmatrix} \qquad (11)$$

The motion parameter vector X, which includes translational displacements and rotational angles, was obtained by solving the matrix equation using the least squares method.

The sampling frequency for solving translational and rotational motion was set to 200 Hz. The corresponding frequency-domain analysis results are shown in Figure 11.

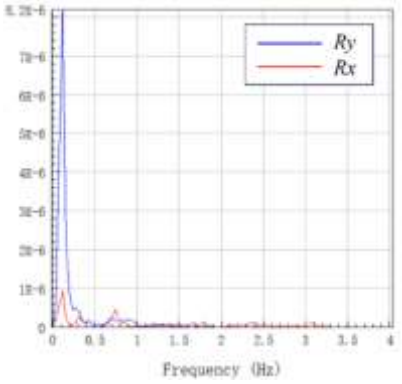

A1. Angle（rad）

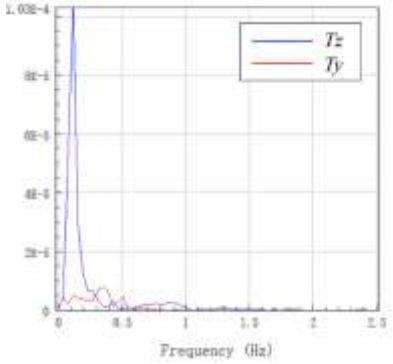

B1. Displacement（m）

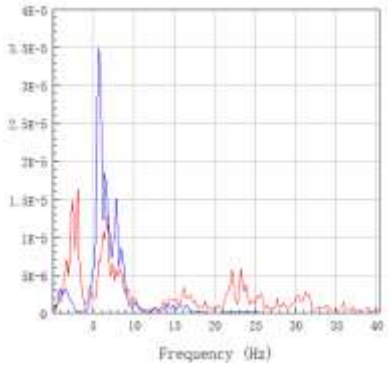

A2. Angular velocity (rad/s)

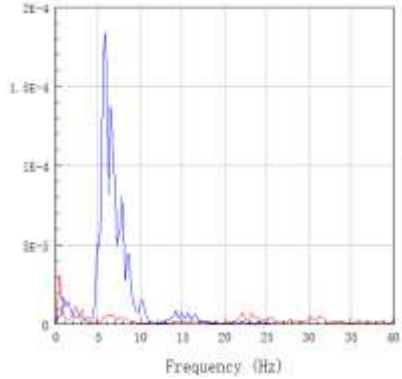

B2. Velocity (m/s)

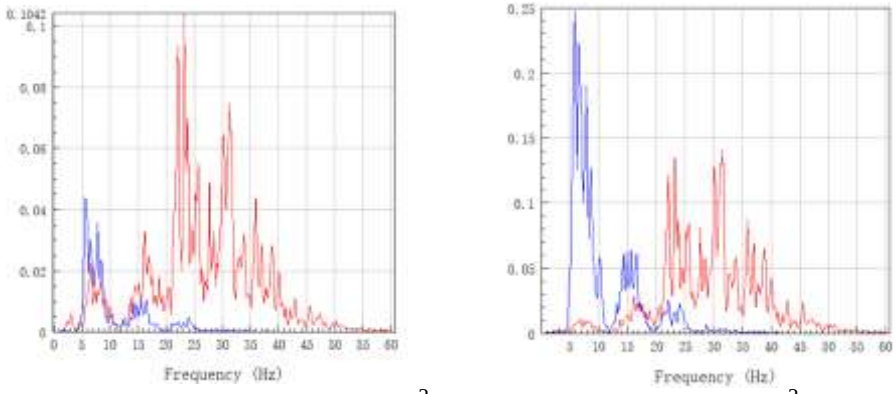

A3. Angular Acceleration (rad/s^2) B3. Acceleration (m/s^2)

Figure 11 Excitation spectrum of the pantograph base

From the frequency spectrum of the pantograph base excitation, it is evident that in the rotational direction, the pitch angle *Ry* dominates in the low-frequency range (< 0.5 Hz), indicating a flexible vehicle response to long-wavelength road undulations. Meanwhile, both the angular velocity and angular acceleration spectra exhibit pronounced peaks in the 6–10 Hz range, corresponding to the vehicle's first-order pitch mode. In contrast, the angular acceleration of the roll angle *Rx* displays multiple peaks between 15–35 Hz, suggesting the presence of high-frequency lateral vibration modes.

In the translational direction, the vertical displacement spectrum *Tz* also exhibits strong low-frequency components. Its velocity and acceleration spectra show peak energy concentrated in the 6–10 Hz band, closely aligned with the rotational pitch modes, indicating a strong coupling between vertical vibration and pitch motion. In contrast, the lateral displacement response *Ty* shows energy concentration in the high-frequency range (> 20 Hz), likely due to lateral excitations originating from the onboard DCDC unit. Overall, the pantograph base demonstrates flexible body behavior at low frequencies, while exhibiting rigid structural dynamics at higher frequencies.

6 Conclusion

(1) A road roughness inverse modeling framework was developed.

A response-based reconstruction method was proposed, leveraging the parameterization capability of the harmonic superposition method. Through segment-wise optimization of road spectrum parameters, the time-domain RMS error between simulated and measured vehicle responses was minimized. This enabled a stepwise approximation and fitting of the real-world road profile, resulting in a spatially consistent and dynamically accurate 3D road roughness model.

(2) The engineering application of the inversion road spectrum in the electrified road system has been achieved.

Based on the road spectrum model obtained through inversion, the vibration and rotation excitation spectra of the vehicle-mounted pantograph base were analyzed. The results show that the pitch angle *Ry* and vertical translation *Tz* dominate the low-frequency range with consistent peak frequencies, indicating strong dynamic coupling. Meanwhile, roll angle *Rx* and lateral translation *Ty* exhibit multi-peak responses in the 20–40 Hz range, likely due to local resonance effects induced by the onboard DCDC unit. This result demonstrates the effectiveness and adaptability of the reconstructed road spectrum model in the study of the dynamics of electrified roads.

Funding: "This research was funded by 1. Research and Development of Key Technologies for Safe and Efficient Power Supply Of The Test And Verification Platform for Electrified Road Transportation Systems，grant number 2024-C303；2.Fundamental Research Funds for Central Public-Interest Scientific Institutions, Talent Development Program (Youth Innovation Project), grant number 2025-9039" , and "The APC was funded by Z.W.".

References

1. Zheng, Z., Liu, H., Li, Y., et al. (2019). Research on electrified road technology. China Journal of Highway and Transport,

32(5), 132–141.
2. Pei, Y., Chen, F., Ma, T., et al. (2024). A comparative review study on the electrified road structures: Performances, sustainability, and prospects. Structures, 62, 106185.
3. Ji, J., Wang, Z., Zhang, R., et al. (2020). Rutting resistance of direct coal liquefaction residue (DCLR) modified asphalt mixture under variable loads over a wide temperature range. Construction and Building Materials, 257, 119489.
4. Ren, H. (2022). Study on rutting development and prediction method of asphalt pavement based on accelerated loading test. Master's thesis, Southeast University.
5. Wang, H., Wang, Q., Rui, Q., et al. (2016). Research on digital modeling method for vehicle running road surfaces. Acta Armamentarii, 37(7), 1153–1160.
6. Qin, Y., Wang, Z., Xiang, C., et al. (2019). Speed-independent road classification strategy based on vehicle response: Theory and experimental validation. Mechanical Systems and Signal Processing, 117, 653–666.
7. Chen, S., Tong, J., Jiang, X., et al. (2020). Modeling method for non-stationary road roughness based on modulated white noise and table lookup. Journal of Traffic and Transportation Engineering, 20(6), 171–179.
8. Yin, J., Chen, X., Wu, L., et al. (2017). Time-domain simulation of filtered white noise road profile and suspension performance. Journal of Tongji University (Natural Science), 45(3), 398–407.
9. Chen, S. A., Li, X. W., & Wang, J. C. (2024). High-order filtering white noises modulated by coherent and incoherent functions based road irregularities. *IEEE Transactions on Intelligent Vehicles*, *9*(2), 3952-3963.
10. Yu, G., Zhou, X., Dong, J., et al. (2020). 3D stochastic road modeling and simulation based on inverse Fourier transform. Journal of Chongqing University, 43(10), 62–69
11. Liang, G., Zhao, T., Shangguan, Z., et al. (2022). Experimental study of road identification by LSTM with application to adaptive suspension damping control. Mechanical Systems and Signal Processing, 177, 109197.
12. Chen, S., Xue, J. (2022). Road roughness level identification based on BiGRU network. IEEE Access, 10, 32696–32705.
13. Zhao, L., Yu, Y., Zhou, C., et al. (2018). A hydraulic semi-active suspension based on road statistical properties and its road identification. Applied Sciences, 8(5), 740.
14. Zhang, Q., Hou, J., Duan, Z., et al. (2021). Road roughness estimation based on the vehicle frequency response function. Actuators, 10(5), 89.
15. Li, G. (2021). Dynamic uncertainty analysis and optimization of heavy-duty tractor under different road excitations. Doctoral dissertation, Northeastern University.